od [A. L. Blum *et al.*, *Gastroenterology* **61**, 189 (1971)]. The underlying muscle layer of the fundic mucosa was removed, and the tissue was incubated for 2 hours with Pronase, collagenase type IV, and bovine serum albumin, each at 1 mg/ml, and 0.1 m*M* cimetidine in a NaCl Ringer solution containing 85 m*M* NaCl, 4 m*M* KCl, 20 m*M* $NaHCO_3$, 1.0 m*M* $CaCl_2$, 1.0 m*M* $MgCl_2$, 1.0 m*M* KH_2PO_4, 5 m*M* glucose, and 10 m*M* Hepes that had been equilibrated with 95% O_2:5% CO_2 to *p*H 7.3. After incubation, the surface cells were removed by blotting the mucosal surface on absorbent paper. The tissue was subsequently shaken in a small volume of NaCl Ringer solution to release the oxyntic cells. The patch-clamp methods used have been described previously (*9*). Gigaohm seals were formed on the apical membranes of isolated oxyntic cells placed in a chamber on the stage of an inverted microscope.

9. S. Ueda, D. D. F. Loo, G. Sachs, *J. Membr. Biol.* **97**, 31 (1987).
10. We studied patches of the apical membrane because it was morphologically distinct (Fig. 1) and because the basolateral membrane of oxyntic cells does not contain a Cl^- conductance as determined from rapid solution-change experiments on cells impaled with microelectrodes across their basolateral membranes in the intact epithelium. Reducing basolateral Cl^- concentration to one-tenth of its normal concentration results in a slight hyperpolarization of the basolateral membrane potential and has no effect on the ratio of apical to basolateral membrane resistances (J. R. Demarest, unpublished data).
11. S. Nakajima, R. L. Shoemaker, B. I. Hirschowitz, G. Sachs, *Am. J. Physiol.* **219**, 1259 (1970).
12. C. Clausen, T. E. Machen, J. M. Diamond, *Science* **217**, 448 (1982).
13. J. R. Demarest and T. E. Machen, *Am. J. Physiol.* **249**, C535 (1985).
14. For example, the intracellular Cl^- activity measured in acinar cells of the rabbit submandibular gland with ion-selective microelectrodes is 42 to 44 m*M* [K. R. Lau and R. M. Case, *Pfluegers Arch.* **411**, 670 (1988)]. If we take −20 mV as the reversal (Nernst) potential for the channel shown in Fig. 2B, the intracellular Cl^- activity in the oxyntic cell would be 42.6 m*M*, assuming an activity coefficient of 0.76 for the Ringer solution and the cell interior.
15. O. H. Petersen, *Am. J. Physiol.* **251**, G1 (1986); R. C. De Lisle and U. Hopfer, *ibid.* **250**, G489 (1986).
16. M. Schwartz, A. D. Pacifico, T. N. Mackrell, A. Jacobson, W. S. Rehm, *Proc. Soc. Exp. Biol. Med.* **127**, 223 (1968); W. L. McLennan, T. E. Machen, T. Zeuthen, *Am. J. Physiol.* **239**, G151 (1980).
17. Supported by Smith Kline Beckman fellowships to D.D.F.L. and J.R.D., NIH grant DK38664 to J.R.D. and NIH grants AM17328 and DK40615 to G.S., and a U.S. Veterans Administration Senior Medical Investigator award to G.S.

13 January 1989; accepted 18 April 1989

The Location of DNA in RecA-DNA Helical Filaments

E. H. EGELMAN* AND X. YU*

The helical filament that the RecA protein of *Escherichia coli* forms around DNA is the active apparatus in protein-catalyzed homologous genetic recombination. The actual position of DNA within this complex has been unknown. Image analysis has been performed on electron micrographs of filaments of RecA on double-stranded DNA and on single-stranded DNA to visualize a difference that is consistent with one strand of the double-stranded DNA. This localization of the DNA gives additional information about the unusual structure of DNA in the complex with RecA protein.

THE RECA PROTEIN OF *Escherichia coli* has been the most extensively studied enzyme of general (homologous) genetic recombination (*1–3*). In in vitro systems this enzyme alone can mediate the recognition and strand exchange between two homologous DNA molecules, the central events in homologous recombination. The biologically active form of the RecA molecule, both in vivo (*4*) and in vitro (*5, 6*), is a polymer, and all available evidence suggests that the structural framework for the strand exchange is a helical polymer of RecA that forms around one DNA molecule that is either single-stranded or has a single-stranded region. Homologous recognition and strand exchange then occur when a homologous DNA molecule is brought into this complex. We report a direct localization of a significant feature that we interpret to be the DNA within the complex initially formed by RecA around a DNA molecule. This observation, based on conventional negative-stain electron microscopy, was made possible by image processing that has revealed a feature (one strand of DNA) that accounts for about 2.5% of the total mass of the complex. The method we have used is both simple and powerful and can readily be applied to other polymeric protein-DNA structures.

RecA filaments were prepared on both single-stranded DNA (ssDNA) and double-stranded DNA (dsDNA) in the presence of a relatively nonhydrolyzable adenosine triphosphate (ATP) analog, ATP-γ-S. Filaments were negatively stained with uranyl acetate, and electron micrographs were taken on film (Fig. 1). Images of more than 100 filament sections (where each filament section was typically from 1500 to 3000 Å long) were scanned with a digital densitometer, corrected for curvature (*7*), and Fourier-transformed. The Fourier transform of the projection of a helical object is nonzero everywhere except on layer lines, where the spacing of the layer lines is related to the pitch of the helices from which they arise (*8*). Three layer lines were extracted from each filament transform (Bessel function order 0, 1, and 2), all arising from the right-handed 95 Å pitch helix in the RecA filament. After filaments with marginal data were excluded, two average data sets were generated: a RecA-ssDNA set from 44 filaments and a RecA-dsDNA set from 39 filaments. The up-down phase residuals (*9*) for each of the individual filaments against the average, which is a measure of both the polarity of the structure and the quality of the data, are shown in Fig. 2. The averaged layer line data were then used to generate the helically projected density distribution of the filament (Fig. 3), which corresponds to a cross section of the filament that has been averaged along the 95 Å pitch helix.

Because the difference between the two data sets has a component that is due entirely to noise (sample statistics) and a component that is physically meaningful but small, we have generated a difference map that is expressed in units of standard errors. To do this, we have determined the standard error of the mean (SEM) at every pixel in each of the two average maps,

$$\mathrm{SEM}_{i,j} = \frac{\left[\sum_{k=1}^{n} (\rho_{i,j}{}^{k})^2 - \left(\sum_{k=1}^{n} \rho_{i,j}{}^{k}\right)^2\right]^{1/2}}{[(n-1)n]^{1/2}} \quad (1)$$

where $\rho_{i,j}{}^{k}$ is the density at point i,j in the kth map. The standard error at every point in the difference map is then:

$$\sigma_{i,j}{}^{\mathrm{dif}} = [(\mathrm{SEM}_{i,j}{}^{\mathrm{ds}})^2 + (\mathrm{SEM}_{i,j}{}^{\mathrm{ss}})^2]^{1/2} \quad (2)$$

The densities in the difference map can then be divided by the standard error at every point in the difference map to show the significance of features. The result is shown in Fig. 3, in which only one strong feature emerges, with a peak value of 4.8 standard errors. This feature is thus quite significant statistically, and we interpret it to be one strand of the dsDNA and not a conformational change of the protein or the staining pattern, for four reasons.

1) Because the DNA in the RecA-DNA complex follows the RecA helix, stereochemical constraints dictate that the axis of the dsDNA cannot be more than 17 Å radially from the RecA filament axis (*10*). The feature that we observed is centered at a radius of about 7 Å, consistent with this constraint.

2) The DNA within the RecA-DNA complex must be accessible to external DNA molecules. Parts of DNA in the complex with RecA can be methylated by dimethyl

Department of Molecular Biophysics and Biochemistry, Yale University, New Haven, CT 06511.

*Present address: Department of Cell Biology and Neuroanatomy, University of Minnesota, Minneapolis, MN 55455.

sulfate (*11, 12*), so the DNA must be located in a partially exposed position within the deep helical groove of the RecA filament. The difference peak is located at the edge of the RecA-dsDNA cross section, consistent with this constraint.

3) We know the stoichiometry of the RecA-dsDNA complex (*13*) (3 bp per RecA) and the RecA molecular weight (*14*), 37,842, so we know that dsDNA accounts for about 5.0% of the total mass of the RecA-dsDNA complex. Thus, one strand of dsDNA would account for about 2.5% of the mass of the RecA-dsDNA filament. Because the density of DNA is almost 50% greater than that of protein, and if negative staining is purely related to volume, then the volume of a single strand would be about 1.7% of the total volume. The total integrated density of the main difference peak that is seen is about 1% of the total integrated density of the RecA-dsDNA map. Because the peak is positive and in good agreement in size with what one would expect from the simplest assumptions, the DNA appears to be simply excluding stain penetration in the same manner as the protein.

4) We have done a series of control experiments that support the view that the differences are real and reproducible. When independently prepared samples of filaments from the same population are compared, no statistically significant differences are seen (data not shown). We have averaged 48 RecA filaments formed on the single-stranded polyribonucleotide poly(rA), and, when this map is compared with the map of RecA on ssDNA (averaged from 44 filaments), the largest difference within the boundaries of the two filaments is only 1.5 standard deviations. Similarly, a sample of 27 RecA filaments on dsDNA was independently prepared and processed. The largest difference that was observed between this average and the previous average of 39 filaments on dsDNA was only 1.6 standard deviations. Thus, the possibility that the difference that we see arises from systematic errors between two different data sets appears unlikely.

Testing this observation by looking at difference maps between RecA self-polymers and both RecA-ssDNA filaments and RecA-dsDNA filaments is not possible, because RecA–ATP-γ-S filaments do not appear to form in the absence of polynucleotides (*15*). We can also not exclude the possibility that the difference is entirely due to a conformational change in the protein between binding ssDNA and dsDNA, but this seems unlikely, given the arguments presented above for why the difference is consistent with DNA. The feature that we see arises from a difference at 1/24 $Å^{-1}$ in the transforms (a peak at a radius in reciprocal space of $R = 0.040$ $Å^{-1}$ on the 1/95 $Å^{-1}$ layer line), so it is consistent with the resolution obtainable by conventional negative stain.

These observations have implications for understanding the RecA-mediated strand

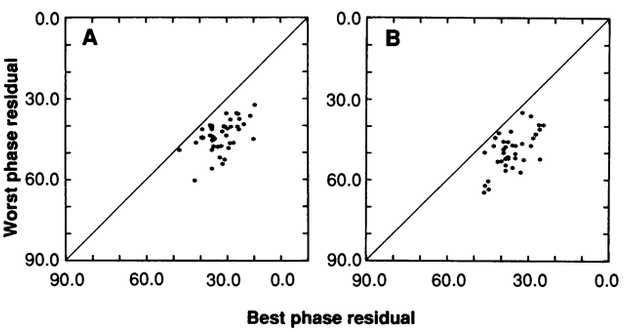

Fig. 2. After the layer line data had been averaged together, an average layer line set was created from 39 RecA-dsDNA filaments and 44 RecA-ssDNA filaments. The layer line data are complex and have both amplitude and phase. The amplitude-weighted phase difference, or residual, in degrees, between each of the individual filaments and the averages are shown [for ssDNA in (**A**) and for dsDNA in (**B**)]. Each filament yields two phase residuals, one for each polarity it is tested with against the average. If the RecA filament were nonpolar or if data were averaged together randomly, points would be grouped along the diagonal line, which is the locus of points having equal residuals for both polarities. For the RecA-ssDNA filaments, the average "best" residual was 32° and the average "worst" residual was 44°. For the RecA-dsDNA filaments, the average "best" residual was 36° and the "worst" residual was 49°.

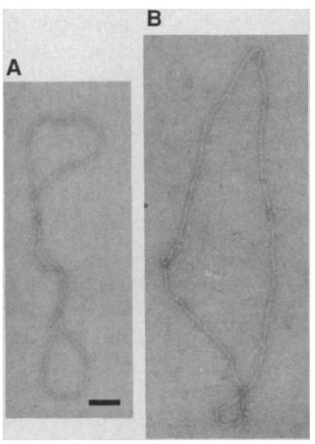

Fig. 1. Electron micrographs of (**A**) RecA-ssDNA filaments and (**B**) RecA-dsDNA filaments. The ssDNA is M13mp8 (7229 bases), whereas the dsDNA is øX174 (5386 bp). Because of residual secondary structure in the ssDNA, which the RecA protein cannot fully melt, the ssDNA in (A) is not fully covered by RecA and thus has a smaller contour length than that of the dsDNA in (B). The two sets of filaments, both prepared with the ATP analog ATP-γ-S, are characterized by a helical pitch of about 95 Å and are indistinguishable to the naked eye. Because RecA unwinds DNA, nicked dsDNA circles were used to allow complete RecA binding. The scale bar is 1000 Å.

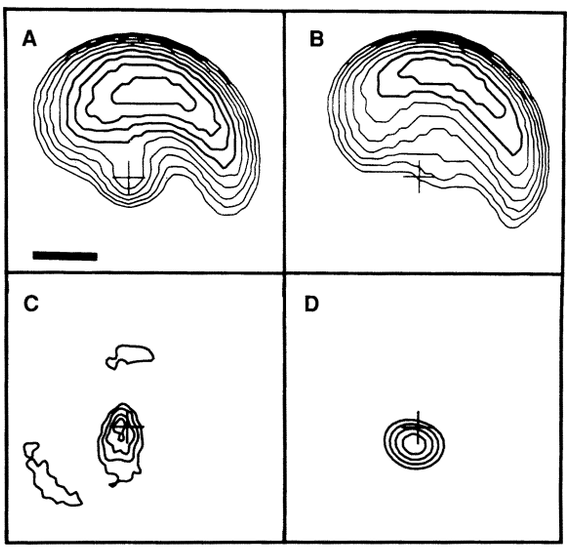

Fig. 3. The three averaged layer lines (layer line numbers 0, 1, and 2, with Bessel orders 0, 1, and 2, respectively) from each of the two sets can be used to generate the helically projected density distributions for (**A**) RecA-dsDNA and (**B**) RecA-ssDNA, where the helical projection is along the 95 Å–pitch right-handed helix. The cross marks the helix axis, and the scale bar is 20 Å. The lowest contour has been chosen to give the correct molecular volume for the filaments. On an arbitrary scale where the peak density in each of these two maps is 60, the largest SEM at any point in the RecA-dsDNA map is 2.2 units and in the RecA-ssDNA map is 1.8 units. The largest error occurs in the RecA-dsDNA map outside of the filament boundary. Because contour steps are 2 units in the scale used, the error in each of these maps is therefore less than one contour step. The difference map, $[(\text{RecA-dsDNA}) - (\text{RecA-ssDNA})]/\sigma^{dif}$, is shown in (**C**) (see text). The contours in (C) are drawn in steps of 0.5 standard error, with the lowest contour at 3 standard errors. The largest peak, interpreted as a single strand of dsDNA, is a difference that has a peak value of 4.8σ. The helical projection in (**D**) is that obtained from a single strand of the dsDNA shown in Fig. 5, B and C, where the two phosphodiester backbones are equidistant from the RecA filament axis. The helical projection in (D) has been created with 20 Å resolution to compare with the real data.

exchange reaction. The localization of the second DNA strand yields more detailed information on the unusual structure of DNA within the RecA filament. Although it has been shown that the axially projected rise per base pair of dsDNA is 5.1 Å in the RecA filament (*16*), the unknown radial position of the DNA strands in the filament has meant that the local rise along the phosphate backbone could be anywhere from 5.1 to 7.6 Å (the stereochemical maximum), because the larger the helical radius of the base pairs, the longer the path length would have to be along the phosphate backbone. The local rise per base pair along the phosphate backbone, α, would be a function of r, the radius of the phosphate backbone:

$$\alpha = [(2\pi r)^2 + 95^2]^{1/2}/18.6 \qquad (3)$$

given that one turn of the 95 Å pitch DNA helix contains 18.6 bp (*13*). The two strands in dsDNA appear to be base-paired in the RecA filament (*12*), and this fact has been incorporated in three schematic dsDNA models in Fig. 4. All these models are consistent with the 5.1 Å projected rise per base pair but have local separations between base pairs along the phosphate backbone of from 5.5 to 7.2 Å. The observed difference peak can be used to distinguish between these models.

Because of the base pairing, the local center of mass between base pairs must be about 5 Å from the center of the difference peak that arises from one of the strands. The ssDNA (and the strand of the dsDNA that is bound to the RecA) would not be located on the side farthest from the protein, so that the local center of mass between the base pairs must be within about 7 Å from the RecA filament axis. Thus, the local rise per base pair along the phosphate backbones in the DNA would be between 5.5 and 5.7 Å. The existence of base pairing suggests that the two strands may be in equivalent geometries, which would require that the center of mass of each strand be at the same helical radius. This would be consistent with the model in Fig. 4C and would exclude the DNA coiling at the larger radii shown in Fig. 4, A and B.

The existence of only one peak in the difference map (ds − ss) shows that one strand of the dsDNA in the RecA filament occupies the same position that ssDNA does. This assumption has been made in certain models for RecA-mediated ss-ds and ds-ds strand exchange reactions (*2*), and our observation provides direct evidence in support of this model.

Because dsDNA within the RecA filament appears to be base-paired (*12*), B-form dsDNA can be untwisted and stretched, as shown in Fig. 5B, to serve as a starting point for understanding the structure of DNA within the RecA filament. We have combined existing data on DNA structure in the RecA-dsDNA filament (*10, 16*) with the new information on the position of DNA to obtain a model (Fig. 5C). The most striking feature of this model is how exposed the base pairs would be to external DNA molecules at the same time that one face of the DNA is completely protected by the RecA protein. A key question has been how the RecA protein mediates recognition between a DNA molecule that is in the extended form shown in Fig. 5B and an external DNA molecule in solution with a form like that shown in Fig. 5A. Recent evidence (*17*) suggests that a second, external DNA molecule is not free in solution but is bound to the RecA protein, independent of homology between the two DNA molecules. RecA protein will then stretch the second DNA molecule, so that the axial rise per base or base pair of both are the same. The deep groove of the RecA helix (Fig. 5C) can easily accommodate a second DNA molecule, as may also be seen in the cross sections of Fig. 3, A and B. Future studies should be directed toward localizing a second DNA molecule when it is taken into the RecA filament.

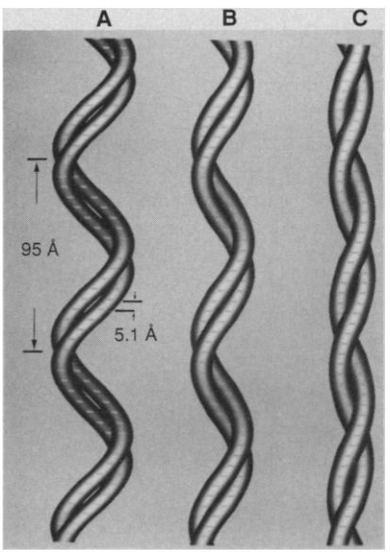

Fig. 4. Three schematic models for the possible arrangement of dsDNA in the complex with RecA. The radius of the solid cylinders, representing the phosphate backbones, is 15 Å in (**A**), 10 Å in (**B**), and 6 Å in (**C**). All three structures would give rise to the observed 5.1 Å axial rise per base pair, but the local separation between base pairs along the phosphate backbone would be 7.2 Å in (A), 6.1 Å in (B), and 5.5 Å in (C).

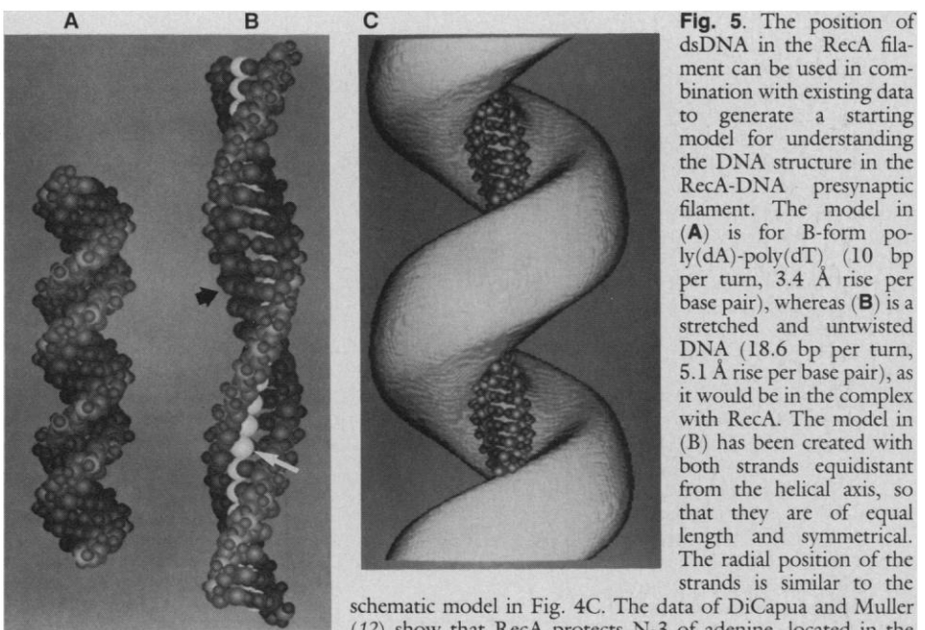

Fig. 5. The position of dsDNA in the RecA filament can be used in combination with existing data to generate a starting model for understanding the DNA structure in the RecA-DNA presynaptic filament. The model in (**A**) is for B-form poly(dA)-poly(dT) (10 bp per turn, 3.4 Å rise per base pair), whereas (**B**) is a stretched and untwisted DNA (18.6 bp per turn, 5.1 Å rise per base pair), as it would be in the complex with RecA. The model in (B) has been created with both strands equidistant from the helical axis, so that they are of equal length and symmetrical. The radial position of the strands is similar to the schematic model in Fig. 4C. The data of DiCapua and Muller (*12*) show that RecA protects N-3 of adenine, located in the minor groove of B-DNA, and shown by the large white atoms in (B) indicated by the white arrow. Dombroski *et al.*, using anthramycin, which binds in the minor groove, came to the same conclusion that RecA binding is along the minor groove (*18*). The major groove, indicated by the black arrow in (B), would be exposed in the RecA-dsDNA complex, shown in (**C**). The filament in (C), which is the surface generated by the helically averaged cross section of RecA on ssDNA shown in Fig. 3B, is oriented with the 3′ end of a resident ssDNA strand at the top, as determined by image analysis (*9*).

REFERENCES AND NOTES

1. C. M. Radding, *Cell* **25**, 3 (1981).
2. P. Howard-Flanders, S. C. West, A. Stasiak, *Nature* **309**, 215 (1984).
3. M. M. Cox and I. R. Lehman, *Annu. Rev. Biochem.* **56**, 229 (1987).
4. S. D. Yancey and R. D. Porter, *Mol. Gen. Genet.* **193**, 53 (1984).
5. S. C. West *et al.*, *Proc. Natl. Acad. Sci. U.S.A.* **77**, 2569 (1980).
6. M. M. Cox and I. R. Lehman, *J. Biol. Chem.* **257**, 8523 (1982).

7. E. H. Egelman, *Ultramicroscopy* **19**, 367 (1986).
8. A. Klug, F. H. C. Crick, H. W. Wyckoff, *Acta Crystallogr.* **11**, 199 (1958).
9. A. Stasiak, E. H. Egelman, P. Howard-Flanders, *J. Mol. Biol.* **202**, 659 (1988).
10. E. H. Egelman and A. Stasiak, *ibid.* **191**, 677 (1986).
11. M. C. Leahy and C. M. Radding, *J. Biol. Chem.* **261**, 6954 (1986).
12. E. DiCapua and B. Muller, *EMBO J.* **6**, 2493 (1987).
13. E. DiCapua, A. Engel, A. Stasiak, Th. Koller, *J. Mol. Biol.* **157**, 87 (1982).
14. A. Sancar, C. Stachelek, W. Konigsberg, W. D. Rupp, *Proc. Natl. Acad. Sci. U.S.A.* **77**, 2611 (1980).
15. X. Yu and E. H. Egelman, unpublished results.
16. A. Stasiak, E. DiCapua, Th. Koller, *J. Mol. Biol.* **151**, 557 (1981).
17. T. Takahashi, M. Kubista, B. Norden, *ibid.* **205**, 137 (1989).
18. D. F. Dombroski, D. G. Scraba, R. D. Bradley, A. R. Morgan, *Nucleic Acids Res.* **11**, 7487 (1983).
19. We thank A. Stasiak and D. DeRosier for helpful discussions. Supported by NIH grant GM35269 and NSF grant DMB 87-12075.

17 February 1989; accepted 10 May 1989

Activators of Protein Kinase C Induce Dissociation of CD4, But Not CD8, from p56^{lck}

TAMARA R. HURLEY, KUNXIN LUO, BARTHOLOMEW M. SEFTON*

The CD4 and CD8 T cell receptor accessory molecules can both be isolated from T lymphocytes in association with p56^{lck}, a membrane-associated, cytoplasmic tyrosine protein kinase that is expressed exclusively in lymphoid cells. The enzymatic activity of p56^{lck} may therefore be regulated by CD4 and CD8 and be important in antigen-induced T cell activation. Exposure of human T cells and some mouse T cells to the tumor promoter 12-O-tetradecanoyl phorbol-13-acetate (TPA), an activator of protein kinase C, caused the dissociation of p56^{lck} and CD4. Activation of protein kinase C may therefore interrupt regulation of p56^{lck} by CD4 and alter the ability of p56^{lck} to interact with polypeptide substrates. In contrast, exposure of cells to TPA did not cause dissociation of p56^{lck} and CD8. Regulation of p56^{lck} by CD4 may therefore differ from regulation by CD8.

THE p56^{lck} PROTEIN IS A MEMBER OF the src family of cellular tyrosine protein kinases (*1*). It is found in essentially all T cells (*1*), where it is presumed to bind to the cytoplasmic face of the plasma membrane. A continuing question has been whether the protein kinases of this family are regulated directly by proteins expressed on the cell surface. The finding that p56^{lck} is physically associated with the T cell accessory molecules CD4 and CD8 (*2*) suggests that its activity may be regulated by these molecules during T cell activation. This is of potential significance in the control of lymphoid cell proliferation and development because expression of constitutively activated p56^{lck} can induce unregulated proliferation of fibroblasts (*3*). In addition, it has been reported that cross-linking of CD4 with antibodies increases the in vitro tyrosine protein kinase activity of p56^{lck} (*4*).

The CD4, CD8, and p56^{lck} proteins all undergo phosphorylation on serine when lymphoid cells are treated with phorbol esters (*5–8*) that are activators of protein kinase C. The functional consequences of these induced phosphorylations are not well understood, although the phosphorylation of CD4 may induce the internalization of this molecule (*5, 6, 9*). We now compare the properties of the complex of CD4 and p56^{lck} with those of the complex of CD8 and p56^{lck}, with particular emphasis on the effects of activation of protein kinase C.

We studied the interaction of CD4 and CD8 with p56^{lck} in HPB-MLT, a human leukemia T cell line (*10*) that expresses both CD4 and CD8 (Fig. 1). At least 30% of p56^{lck} is in association with CD4 and at least 10% is in association with CD8 in this cell line (Fig. 1C). An immunoprecipitate prepared from these cells with the OKT4 antibody to CD4 (anti-CD4) was assayed for protein kinase activity by incubation with [γ-^{32}P]-labeled adenosine triphosphate (ATP). Incorporation of ^{32}P into p56^{lck} (*11*) (Fig. 1A, lane 3) and into an exogenous substrate, acid-denatured enolase (Fig. 1B, lane 3), was observed. In contrast, no labeling of p56^{lck} (Fig. 1A, lane 4) and much reduced labeling of enolase (Fig. 1B, lane 4) were detected when a similar immunoprecipitate from cells that had been exposed to 12-O-tetradecanoyl phorbol-13-acetate (TPA) for 15 min was examined, the level of immunoprecipitated kinase activity being reduced seven- to tenfold. This effect of TPA was probably due to activation of protein kinase C. Treatment of cells with dimethyl sulfoxide (DMSO) (the solvent in which TPA was dissolved) or with 4-β-phorbol (an analog of TPA that does not activate protein kinase C) was without effect (*12*). Conversely, treatment with the synthetic activator of protein kinase C, 1-oleoyl-2-acetylglycerol, had an effect similar to that of TPA (*12*).

The reduced p56^{lck} protein kinase activity associated with CD4 in cells treated with TPA was not caused by loss of p56^{lck} after TPA treatment. Neither the precipitation of p56^{lck} with a rabbit antiserum to p56^{lck} (anti-p56^{lck}) (*13*) (Fig. 1A, lane 8) nor the protein kinase activity of p56^{lck} (Fig. 1B, lane 8) was inhibited by treatment with TPA. However, the gel mobility of p56^{lck} was altered markedly. Approximately 30 to 50% of the p56^{lck} from TPA-treated cells that became labeled with ^{32}P in vitro migrated with an apparent molecular size of 60 to 65 kD (Fig. 1A, lane 8). The retarded gel mobility results from the increased phosphorylation of the protein on serine (*14*) and threonine (*15*) residues. The reduced precipitation of p56^{lck} by OKT4 was also not due to inhibition of the precipitation of CD4 by TPA treatment. Exposure of cells for 10 min to TPA did not affect the immunoprecipitation of CD4 that had been labeled by cell-surface iodination (*12*).

Analysis of the same immunoprecipitates by protein blotting with anti-p56^{lck} antibodies showed that the precipitation of p56^{lck} by OKT4 was undetectable after the exposure of the cells to TPA (Fig. 1C, lane 4). The lack of labeling of p56^{lck} during incubation with ATP in vitro therefore was not the result of inactivation of the protein but rather the result of dissociation of the complex of CD4 and p56^{lck}. We have also examined the effect of the treatment of T cells with TPA on the association of p56^{lck} with CD4 in two other human leukemia T cell lines, VB (*16*) and D-CEM. In both, treatment with TPA induced an almost complete dissociation of CD4 and p56^{lck} in less than 30 min (*12*).

Identical protein kinase assays of immunoprecipitates prepared from HPB-MLT cells with the OKT8 antibody to CD8 (anti-CD8) showed relatively weak labeling of p56^{lck} by autophosphorylation (Fig. 1A, lane 5). Protein blot analysis with anti-p56^{lck} antibodies showed that p56^{lck} was present in the anti-CD8 immunoprecipitates (Fig. 1C, lane 5) at a threefold lower concentration than in OKT4 immunoprecipitates (Fig. 1C, lane 3). The p56^{lck} associated with CD8 was, however, active in the phosphorylation of enolase (Fig. 1B, lane

T. R. Hurley and B. M. Sefton, Molecular Biology and Virology Laboratory, The Salk Institute, P.O. Box 85800, San Diego, CA 92138.
K. Luo, Molecular Biology and Virology Laboratory, The Salk Institute, P.O. Box 85800, San Diego, CA 92138, and Department of Biology, University of California, San Diego, CA 92093.

*To whom correspondence should be addressed.